University of Dundee

CHD pile performance, part II

Knappett, Jonathan; Caucis, Karlis; Brown, Michael; Jeffrey, John Ross; Ball, Jonathan David

CHD pile performance: part II – numerical modelling

[1] Jonathan Adam Knappett MA, MEng, PhD
Reader, School of Science & Engineering, University of Dundee,
Dundee, UK

[2] Karlis Caucis MEng
Graduate Engineer, Arup, South Queensferry, UK (formerly University
of Dundee, Dundee, UK)

[3] Michael John Brown BEng, PhD
Senior Lecturer, Division of Civil Engineering, University of Dundee,
Dundee, UK (corresponding author: m.j.z.brown@dundee.ac.uk)

[4] John Ross Jeffrey MEng, PhD
Graduate Engineer, Technip UK Ltd, Westhill, UK (formerly University
of Dundee, Dundee, UK)

[5] Jonathan David Ball BSc, CGeol, FGS
Chief Geotechnical Engineer, Roger Bullivant Ltd, Burton Upon Trent,
UK
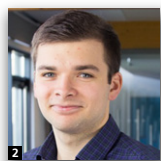
A set of simple finite-element modelling procedures that can be used to estimate the load–settlement behaviour of continuous helical displacement (CHD) piles in sand is presented. The approach makes use of a stress- and strain-dependent non-linear soil model that can be parameterised using basic soil data that can be determined through routine site investigation. The procedures are validated against a database of physical model tests (reported in a companion paper), where they are shown to be suitable for estimating the load–settlement behaviour of CHD piles within the serviceability range. In this way they are complementary to the analytical method reported in the companion paper for estimating the ultimate capacity of a CHD pile. In this paper, the finite-element method and analytical model are applied to four historical load tests on CHD piles conducted at three different sand sites. The modelling is further validated and used to discuss potential savings in pile material and therefore cost due to additional confidence in performance determination at both ultimate and serviceability limit states.

Notation

c'	apparent cohesion
D	pile diameter
D_{core}	continuous helical displacement (CHD) pile core diameter
D_f	CHD pile outer flight (flange) diameter
D_r	relative density of soil
D_{tip}	CHD tip diameter
E_{50}^{ref}	secant Young's modulus at 50% deviatoric failure stress (at p_{ref})
E_{oed}^{ref}	one-dimensional confined Young's modulus (at p_{ref})
E_{ur}^{ref}	elastic unload–reload Young's modulus (at p_{ref})
G_0	(small-strain) shear modulus
G_0^{ref}	reference small-strain shear modulus at p_{ref}
K	coefficient of lateral earth pressure
L	pile length
m	stiffness exponent
N_q	bearing capacity factor
p_{ref}	reference confining pressure (= 100 kPa)
Q_b	pile base load component
Q_{bu}	pile base capacity
Q_s	pile shaft load component

Q_{su}	pile shaft capacity
Q_t	pile head (total) load = $Q_b + Q_s$
Q_{tu}	pile bearing capacity = $Q_{bu} + Q_{su}$
q_c	cone penetration test (CPT) cone resistance
R_f	deviatoric stress failure ratio
R_{inter}	interface friction coefficient
w	pile settlement
z	penetration depth
γ	unit weight of dry soil
δ_{crit}	interface friction angle (critical state)
ε_s	shear strain
$\varepsilon_{s,0\cdot7}$	deviatoric shear strain (at $G/G_0 = 0\cdot7$)
ν_{ur}	Poisson's ratio for elastic unload–reload
σ_v'	vertical effective stress
σ_3'	minor principal stress
ϕ'	angle of internal friction
ϕ_p'	peak angle of friction
ψ'	angle of dilation

1. Introduction

The authors' companion paper (Jeffrey *et al.*, 2016) described the continuous helical displacement (CHD) pile type and

presented a series of small-scale (1*g*) model tests that were conducted to obtain insight into its installation/formation and performance under vertical compressive loading. It was shown that CHD piles in coarse-grained soils can have a similar or better bearing capacity than a displacement-type pile of the same outer diameter, while saving material (due to its screw-type shape and hence variable cross-sectional diameter).

Based on a database of test data derived from model pile installation and load testing in sands across a wide range of relative densities, the companion paper developed values of the bearing capacity factor (N_q) and lateral earth pressure coefficient (K) for use in standard analytical approaches for design at the ultimate limit state. It was proposed that N_q can be used in conjunction with the CHD core diameter (D_c) for determining the base capacity, while K is used with the exterior flange diameter (D_f) and the soil–soil friction angle (rather than the soil–concrete interface friction angle) to determine the shaft capacity.

The analytical approach and factors so derived in the companion paper are useful in preliminary sizing of piles to provide a certain margin of safety against failure. However, under modern limit state design codes (e.g. Eurocode 7 (BSI, 2004)), verification of performance at the serviceability limit state is also recommended. For a pile carrying compressive vertical loading, this consists of meeting limiting settlement criteria on individual piles. For CHD piles, the prediction is complicated by the changes to the near-field soil parameters induced by the formation process. This issue will be addressed in this paper by outlining simple approximate procedures for modelling CHD pile performance under vertical loading using finite-element modelling (FEM), which can subsequently be used both to estimate the load–settlement behaviour and to verify the vertical capacity of the pile determined using the analytical approach from the companion paper.

A key feature of this approach is the use of an advanced non-linear constitutive model for the soil that only requires routinely available site investigation data (i.e. relative density) as an input parameter, to enable widespread use in routine design. The use of relative density to parameterise the soil model also permits installation effects to be taken into account in an approximate way, based on apparent changes to soil density around the pile inferred from cone penetration test (CPT) measurements close to the model piles following installation, the data for which can be found in the companion paper (Jeffrey *et al.*, 2016). The constitutive model incorporates stress-dependent stiffness parameters, and so can be validated against the physical model load–displacement test data prior to failure taken from the companion paper and also applied to full-scale field cases. Following validation against the model tests, the FEM (and the analytical capacity method) are subsequently applied to the prediction of a series of pile load tests from three different field sites around the UK, extracted from

a larger database for CHD piles in a range of soil types developed by Roger Bullivant Ltd, UK.

Finally, it will be shown that the use of the analytical method and FEM can allow designers to produce more efficient CHD pile designs in sands (i.e. confidently utilise a larger proportion of the available capacity and thereby reduce required pile lengths).

2. Constitutive modelling

All of the FEM described in this paper used an elasto-plastic soil model with isotropic hardening (Schanz *et al.*, 1999) in which the elastic behaviour incorporates strain- and stress-dependent stiffness variation, the small-strain stiffness being capped at G_0. This model is available in the Plaxis FEM software as the 'Hardening soil model with small-strain stiffness'. A similar model without the small-strain stiffness cap has previously been used by Tolooiyan and Gavin (2013) to model the behaviour of bored piles in dense sand. Strain dependency is modelled following the model proposed by Hardin and Drnevich (1972), as modified by Santos and Correia (2001)

1. $$\frac{G}{G_0} = \frac{1}{1 + 0.385 \left| \varepsilon_s / \varepsilon_{s,0.7} \right|}$$

where ε_s is the current shear strain and $\varepsilon_{s,0.7}$ is the shear strain at which G/G_0 is 70%. Stress-dependency is modelled through the determination of G_0 for the appropriate confining stress in the soil element

2. $$G_0(\sigma_3') = G_0^{ref} \left(\frac{c' \cos \varphi' - \sigma_3' \sin \varphi'}{c' \cos \varphi' + p_{ref} \sin \varphi'} \right)^m$$

where G_0^{ref} is the small-strain stiffness at a reference pressure $p_{ref} = 100$ kPa, σ_3' is the minor principal stress and m is an exponent modelling the variation of stiffness with stress level ($m \approx 0.5$ is typical in sands (e.g. Oztoprak and Bolton, 2013)). Plastic failure is modelled using a cap-type yield surface combined with the Mohr–Coulomb failure criterion.

The model requires 13 input parameters

- unit weights under saturated and dry conditions (these are the same for dry sand)
- three measureable effective stress peak strength parameters – peak angle of friction (φ_p'), apparent cohesion (c') and angle of dilation (ψ') – for use in the Mohr–Coulomb failure criterion
- six measurable stiffness parameters (defined at $p_{ref} = 100$ kPa) describing the response to deviatoric loading (E_{50}^{ref}), compressive loading (E_{oed}^{ref}), unload/reload cycles (E_{ur}^{ref}, ν_{ur}), small-strain stiffness (G_0^{ref}) and shear strain for describing the shape of the $G - \varepsilon_s$ relationship ($\varepsilon_{s,0.7}$)

■ two empirical parameters R_f and m, the former of which controls the deviatoric stress at failure (providing a defined limiting capacity to what is otherwise a hyperbolic stress–strain relationship) and the latter controls the variation of the stiffness parameters with effective confining stress (e.g. variation with depth).

Although the model has a number of input parameters, it should be noted that all but R_f and m can be directly measured in some form through routine laboratory testing.

Two sets of material parameter correlations were used in the work described in this paper. Brinkgreve *et al.* (2010) presented a set of relationships for determining the aforementioned parameters in sands as a function of relative density (D_r), based on a collation of triaxial and other test data from a range of sands reported in the literature. Subsequently, Al-Defae *et al.* (2013) produced a set of soil-specific correlations for the HST95 sand used in the model tests reported in the companion paper (Jeffrey *et al.*, 2016). The model parameters have subsequently been validated against centrifuge test data (i.e. full-scale stresses) on the dynamic response of sandy slopes (Al-Defae *et al.*, 2013; Liang *et al.*, 2015) and buildings on shallow foundations (Knappett *et al.*, 2015) during earthquake shaking. The use of the correlations in this paper allows for an additional validation to be made against 1g test data (to explore the stress dependency of stiffness) and for a static loading problem. Table 1 summarises the correlations used in the two parameter sets.

As the main focus of this paper is prediction of load–settlement of piles at loads below ultimate bearing capacity, Figure 1 shows some of the key stiffness related parameters for the two parameter sets (E_{oed}^{ref} and m), along with other soil-specific values for other specific sands collated by Tolooiyan

and Gavin (2013). A key observation from this figure is that the HST95 correlation is significantly stiffer than the Brinkgreve *et al.* (2010) correlation in looser soils (particularly for $D_r < 45\%$) and less stiff in denser soils. Given that a key part of this study was the modelling of piles at both 1:10 and 1:1 scales and therefore different stress levels, the two correlations were used to simulate numerically oedometer tests on dry HST95 sand at three contrasting relative densities close to those considered in the model tests of the companion paper, over a wide range of stress increments between 0–600 kPa. This used a simple two-dimensional axisymmetric FEM of the oedometer test cell. The simulation results in Figure 2 are consistent with the observations from Figure 1 in that the Brinkgreve *et al.* (2010) correlation significantly under-predicts the stiffness of the soil at a loose state ($D_r = 18\%$) and over-predicts the stiffness under very dense conditions ($D_r = 83\%$).

Parameter	Brinkgreve *et al.* (2010)	HST95 (Al-Defae *et al.*, 2013)
ϕ_p': degrees	$12 \cdot 5D_r + 28$	$20D_r + 29$
c': kPa	0	0
ψ': degrees	$12 \cdot 5D_r - 2$	$25D_r - 4$
E_{oed}^{ref}: MPa	$60D_r$	$25D_r + 20 \cdot 22$
E_{50}^{ref}: MPa	E_{oed}^{ref}	$1 \cdot 25E_{oed}^{ref}$
E_{ur}^{ref}: MPa	$3E_{oed}^{ref}$	$3E_{oed}^{ref}$
ν_{ur}	$0 \cdot 2$	$0 \cdot 2$
G_0^{ref}: MPa	$68D_r + 60 \cdot 00$	$50D_r + 88 \cdot 80$
$\varepsilon_{s,0 \cdot 7}$	$2 - D_r \, (\times 10^{-4})$	$1 \cdot 7D_r + 0 \cdot 67 \, (\times 10^{-4})$
R_f	$1 - 0 \cdot 13D_r$	$0 \cdot 9$
m	$0 \cdot 7 - 0 \cdot 31D_r$	$0 \cdot 6 - 0 \cdot 1D_r$
γ: kN/m³	$4D_r + 15 \cdot 0$	$3D_r + 14 \cdot 5$

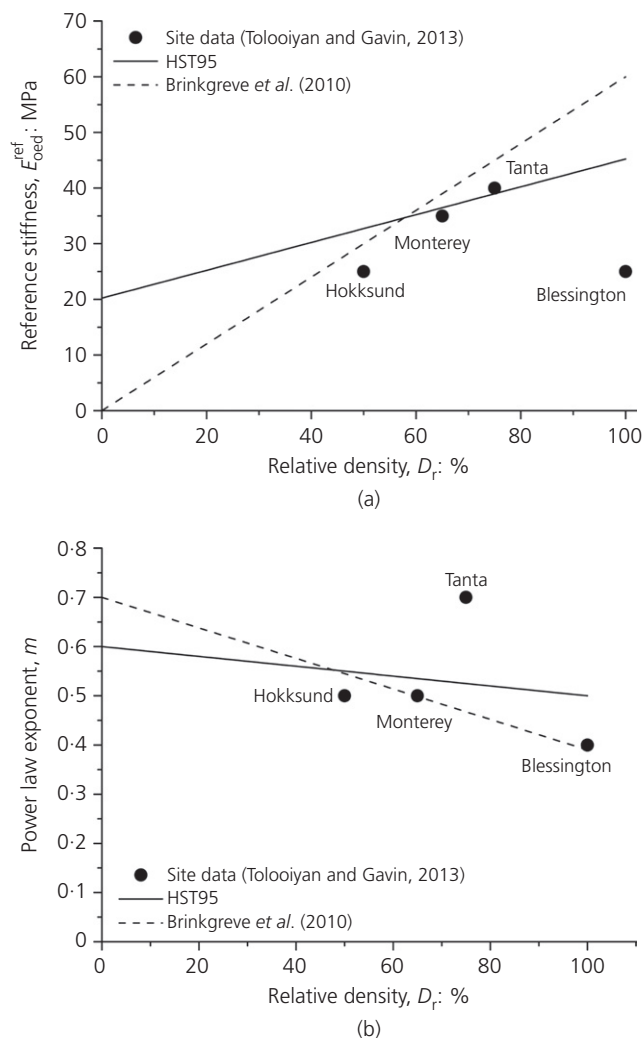**Table 1.** Constitutive model parameter sets

Figure 1. Key non-linear soil stiffness parameters used in numerical modelling: (a) oedometric stiffness at $p_{ref} = 100$ kPa; (b) exponent for stiffness variation with effective confining stress
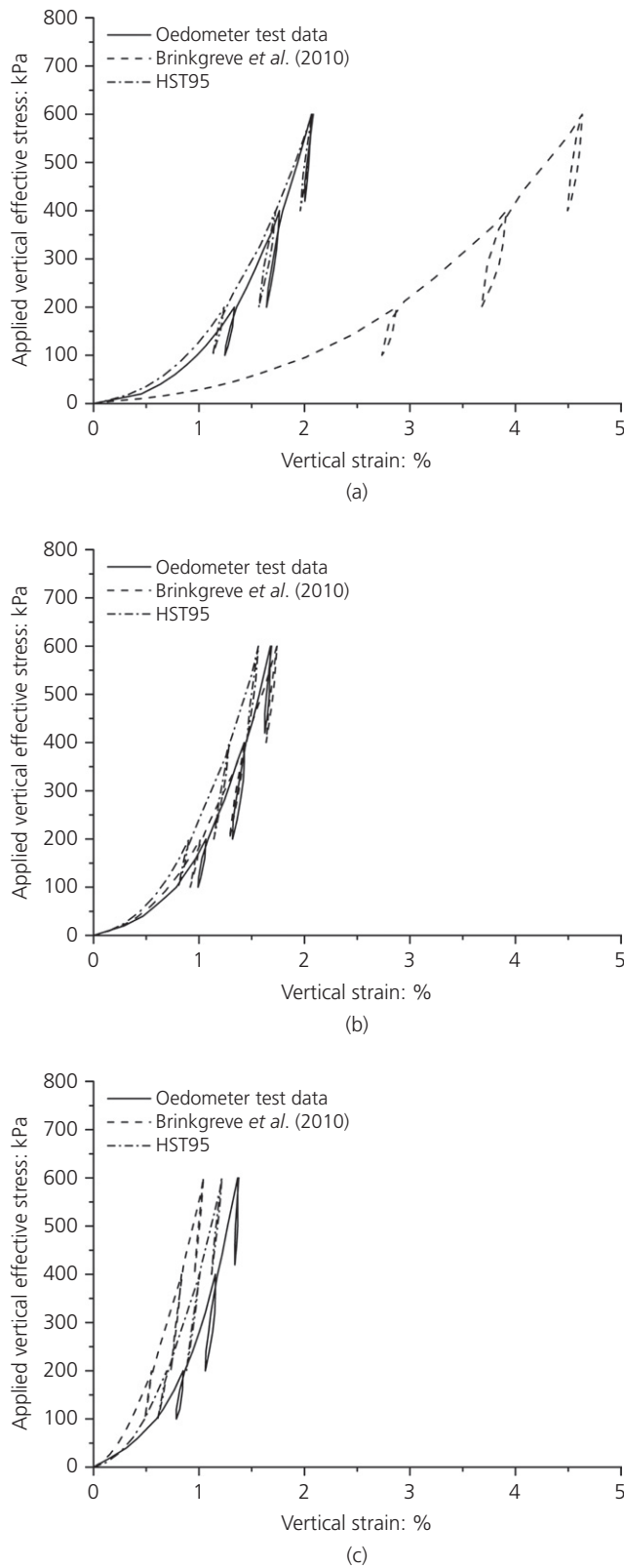
Figure 2. Performance of different parameter correlations in oedometric compression: (a) $D_r = 18\%$; (b) $D_r = 49\%$; (c) $D_r = 83\%$
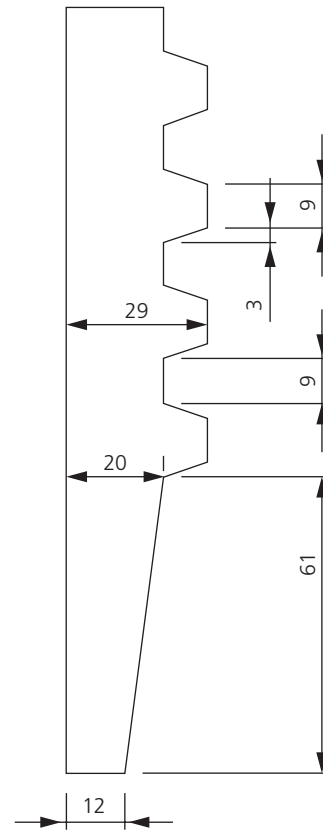

Figure 3. CHD pile geometry used in FEM of model CHD piles (dimensions in mm)

At a medium dense state, the two correlations show very similar behaviour. In addition to a good match at lower stresses, the HST95 model provides a reasonable prediction of non-linear stiffness at higher stresses consistent with full-scale conditions, though the match is best in looser soil, with a small under-prediction in medium dense conditions and a small over-prediction for dense conditions.

3. Application of FEM to small-scale model tests

3.1 General modelling considerations

Figure 3 shows the geometry of half of a CHD pile that was used in all cases in the FEM to simulate the 1:10 scale model tests reported in the companion paper (Jeffrey *et al.*, 2016). This represents an idealisation (averaging) of measurements taken for all of the physical CHD models following exhumation after the load testing. Figure 4 shows the model domain and the mesh of triangular 15-node elements used, the pile being modelled axisymmetrically. The overall width of the model domain (including half the pile diameter) was $7D_f$, where D_f is the outer (flange) diameter of the pile. This is slightly less than the $7·5D$ width used by Tolooiyan and Gavin (2013) but larger than the width of $5D$ used by Kurian and
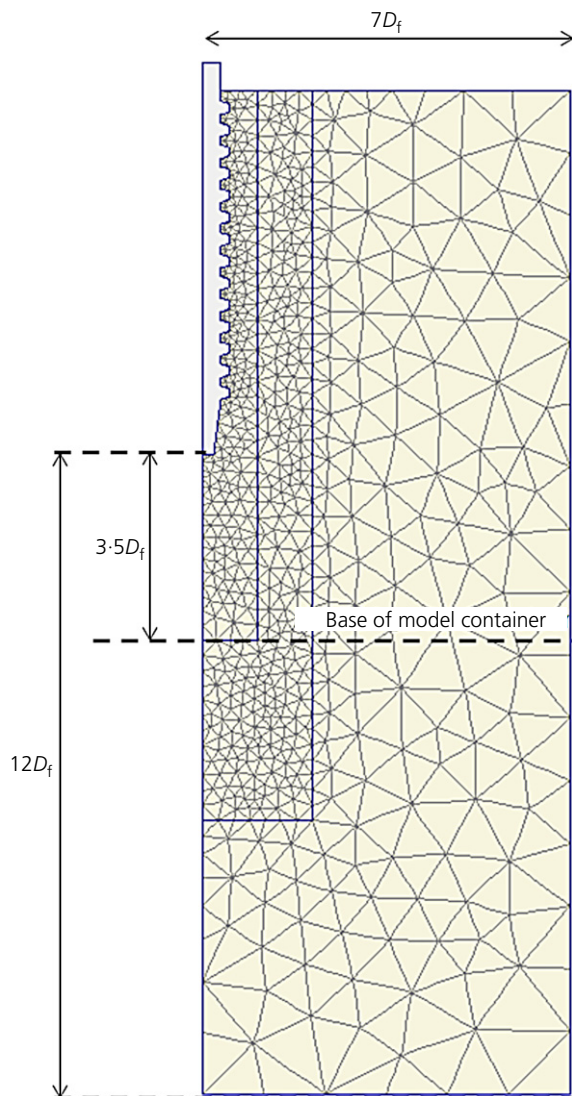
Figure 4. Model domain and mesh configuration for FEM of a model CHD pile

Figure 5. Effect of container boundary on CHD pile performance ($D_r = 59\%$ shown)

there is a negligible difference between the 'semi-infinite' ($12D_f$ boundary) and 'model container' ($3 \cdot 5D_f$ boundary) cases. Referring to the geometry shown in Figure 3, the CHD pile as cast has a very elongated tip, which reduces to a small tip diameter ($D_{tip} = 0 \cdot 4D_f$). If tip behaviour is controlled by this smaller diameter, then the boundary of the model container is actually $3 \cdot 5/0 \cdot 4 = 8 \cdot 75D_{tip}$ from the base of the pile, which would explain the negligible effect of the closer model container boundary in Figure 5. This is also consistent with the use of the smaller core diameter when estimating base capacity in the analytical model presented in the companion paper, and is further supported by Kurian and Shah (2009) who found no boundary effects when the boundary was $> 3D_f$ below the pile tip.

The soil domain was initially partitioned into three zones (see Figure 4): the first zone, closest to the pile had a width of $1D_f$ from the pile centreline; the second extended radially by an additional $1D_f$ from the first zone; the final zone, furthest from the pile, extended to the soil boundaries. The radial locations of the partitions were determined based on the radial distance away from the CHD piles at which post-installation CPTs were conducted for the model CHD piles. The mesh density was increased in the zones closer to the pile where the stresses and strains will show a greater variation over short distances. Wehnert and Vermeer (2004) suggest that at least three elements should be provided beneath the tip of a pile to avoid mesh dependency; it can be seen from Figure 4 that this is satisfied for both of the lower boundary conditions used. Figure 5 also includes a simulation using a coarser mesh than that shown in Figure 4. The coarser mesh had approximately half the number of elements (i.e. the element size was 40% bigger in the x- and y-directions on average). This shows a negligible difference to the cases using the fully refined mesh, suggesting that the mesh had been refined sufficiently to minimise mesh dependency.

Shah (2009). From these previous studies it can be inferred that there is no unwanted radial boundary effect when the domain width is greater than 5D. In the vertical direction, models were produced having (a) a rigid boundary at the actual depth of the model container used in the physical tests (i.e. $3 \cdot 5D_f$ of soil beneath the pile tip) and (b) $12D_f$ of soil below the tip (as an approximation of a semi-infinite half-space). Figure 5 shows a comparison of the load–settlement behaviour for a model CHD pile in medium dense soil (model pile CHD 103, $D_r = 59\%$). The settlement is normalised by the pile diameter ($D = D_f$) and the results are plotted to 10% of the outer diameter (i.e. $w \leq 0 \cdot 1D$), at which point the ultimate bearing capacity of the pile was assumed to have been reached. In addition to the generally good match between the measured and numerically simulated behaviour, it can be seen that
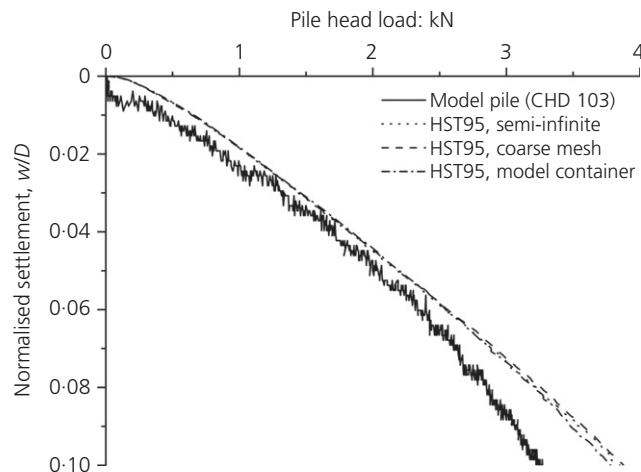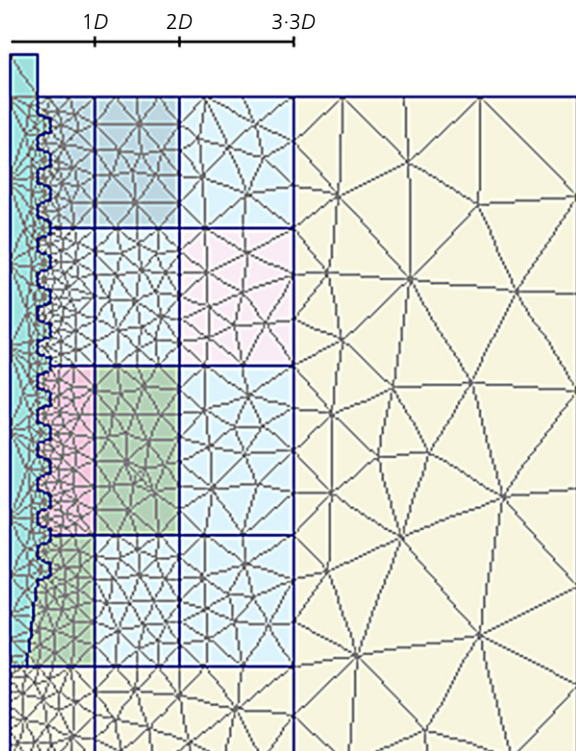
Figure 6. Partitioning of the FE mesh to allow for modelling of radial and vertical variation in soil density due to CHD installation

All of the soil was initially modelled using the correlations in Table 1 based on the pre-test (i.e. in situ) measurements of relative density (which was uniform with depth). Interface elements were also incorporated between the soil and the ribbed shaft of the pile, with a coefficient of friction $R_{inter} = \tan \delta_{crit}$, where δ_{crit} was the critical state (large-strain) concrete–soil interface friction angle reported in the companion paper (Jeffrey *et al.*, 2016). The pile load test was simulated by applying a downwards vertical displacement at the pile head (i.e. under displacement control). The resulting stress distributions induced by this deformation within the top and across the base of the pile were then numerically integrated to determine the overall pile head load and the base load component, respectively. The shaft load component was then determined as the difference between these two measurements.

3.2 Consideration of installation effects

Post-test CPT measurements reported in the companion paper (Jeffrey *et al.*, 2016) suggested that there are potentially significant changes to the soil state around a CHD pile following installation. These would involve changes to the soil density and horizontal stresses due to cavity expansion and contraction during the various installation stages. Changes to lateral stress in dry sand models are difficult to estimate. The soil will expand and then contract back as the bullet passes in the downwards direction, followed by re-expansion as the bullet is retracted and replaced by wet concrete. As the concrete sets

there is only a relatively small difference between the unit weights of the fresh cementitious grout (~ 24 kN/m^3) and sand (15–17 kN/m^3), which will likely result in some lateral stress relaxation within the surrounding sand after the bullet has passed. Indeed, exhumed model piles all exhibited fresh sand embedded within the model pile's surface. This would suggest that the value of the lateral earth pressure coefficient K may be anywhere between K_0 and values for displacement piles (e.g. $K_0 \leq K \leq 2K_0$ (Kulhawy, 1984)). As the model piles were cast in situ, it was not possible to install earth pressure cells to measure the horizontal stress changes. In the interests of developing a simplified set of approximate modelling procedures, lower bound estimates of K were assumed (i.e. K_0 conditions) in all soil zones shown in Figure 4. If $K > K_0$, the FEM simulations will under-predict the loads on the pile due to lower shaft friction.

Apparent density changes, however, could be investigated in an approximate way by post-test CPT probes close to the installed model piles (see the companion paper (Jeffrey *et al.*, 2016)). The post-installation CPT probes suggested that the apparent post-installation density close to the pile varied with depth and radial distance from the pile. This was approximated in the FEM simulations by subdividing the soil mesh close to the pile into four equal-length vertical clusters within each diameter band (Figure 6), within which a single set of constitutive parameters was assumed to apply, determined according to the average post-installation relative density inferred in that zone, as described in the companion paper. The averaged densities used for the loose, medium and dense FEM simulations are shown in Figures 7(a)–7(c), respectively.

The apparent changes in relative density in Figure 7 were inferred by assuming that the post-installation CPTs could be interpreted using $D_r - q_c$ relationships for penetration into virgin soil; that is, there is no change in soil stress state due to model pile installation and that the CPT diameter is small enough that there is no effect of the adjacent pile acting as a rigid boundary constraining the soil deformation mechanism beneath the pile tip. These assumptions are consistent with the assumption of K_0 conditions around the CHD pile shaft described earlier in the paper and may be categorised as an approach in which installation effects are incorporated into a single parameter (local D_r). If the lateral stresses did increase above K_0 and these stresses could hypothetically be incorporated within the CPT interpretation, then the actual relative densities would be lower for the same value of q_c in the enhanced-K soil. Therefore, K would increase but density (and hence mobilised friction angle) would reduce, thereby at least partially cancelling each other out in terms of mobilised shaft resistance at a particular amount of deformation, and likely resulting in similar load–deformation behaviour compared with the adopted approach (lumping the installation effects into local D_r changes). The advantages of the adopted approximate model are that it uses value(s) of K that can be easily determined in practical cases from the soil friction angle and existing $q_c - D_r$ relationships; the alternative method
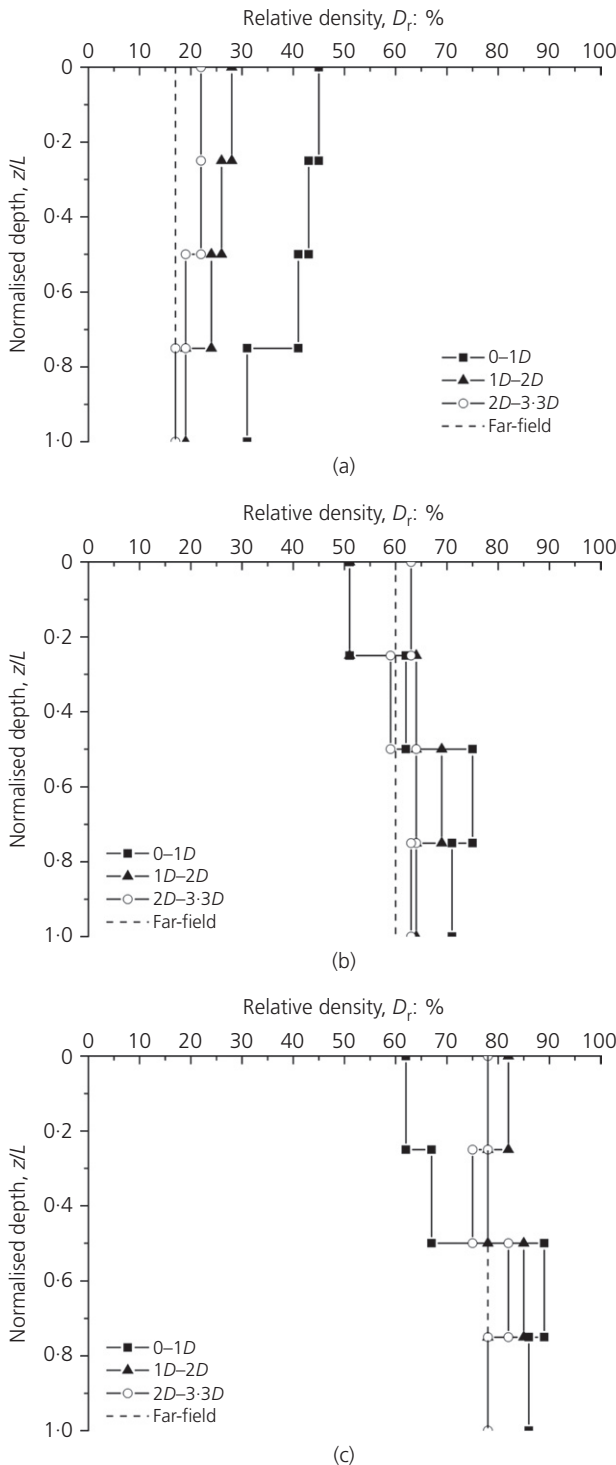
Figure 7. Average post-installation relative density used for the partitions in the FEM: (a) loose sand; (b) medium dense sand; (c) dense sand

described earlier (where K and local D_r both change) requires stress measurements that could not be made and a $q_c - D_r$ interpretation method that does not exist. It should be noted

that the approach adopted here has been previously adopted by Katzenbach and Schmitt (2005) in FEM simulations of auger displacement piles.

3.3 Analytical prediction of pile capacity

Predictions of pile bearing capacity were made in each case for comparison with the load at $w/D = 0.1$ from the FEM simulations and 1g model tests. This used the analytical model outlined in the companion paper (Jeffrey *et al.*, 2016). Shaft capacity was determined in each d$z = 1$ m layer using

$$3. \qquad Q_{su} = \sum_{\text{All layers}} K \cdot \sigma'_v(z) \cdot \tan \phi'_p \cdot \pi D_f \, dz$$

where d$z = 1$ m, $D_f = 0.058$ m from Figure 3 and

$$4. \qquad K = 0.09 e^{0.08 \phi'_p}$$

Base capacity was determined using

$$5. \qquad Q_{bu} = N_q \cdot \sigma'_v(L) \cdot \frac{\pi D_{core}^2}{4}$$

where, from Figure 3, $D_{core} = 0.040$ m and

$$6. \qquad N_q = 1.33 e^{0.11 \phi'_p}$$

In Equations 3 to 6, ϕ'_p is the peak friction angle of the in situ soil (i.e. as measured during initial ground investigations). This therefore represents the opposite approach to the FEM, namely lumping all of the installation effects into an altered value of K (Equation 4) and leaving the friction angle unchanged (i.e. using densities consistent with in situ conditions).

3.4 Validation against model test data

Figure 8 shows predicted (FEM) and measured head load–settlement curves for the model CHD pile in loose sand ($D_r = 17\%$), medium dense sand ($D_r = 59\%$) and dense sand ($D_r = 78\%$) using different modelling assumptions. For the loosest and densest cases (Figures 8(a) and 8(c)), repeat model test results were available; in the medium dense case (Figures 8(b)) only one model curve is shown, as the other piles tested were observed to have forming defects on exhumation and so were excluded from the validation. Use of the Brinkgreve *et al.* (2010) parameter set appears to result in an underestimation of pile stiffness at the low stress levels of the 1g model tests in all cases, though this is most pronounced for the loosest soil, which is consistent with the observations on soil stiffness for these correlations in Figure 1. The FEM simulation using the apparent changes in density from Figure 7 (referred to in Figure 8 as 'HST95 + density change') shows a reasonably good prediction of the overall load–settlement behaviour of the pile, particularly in terms of its shape, though
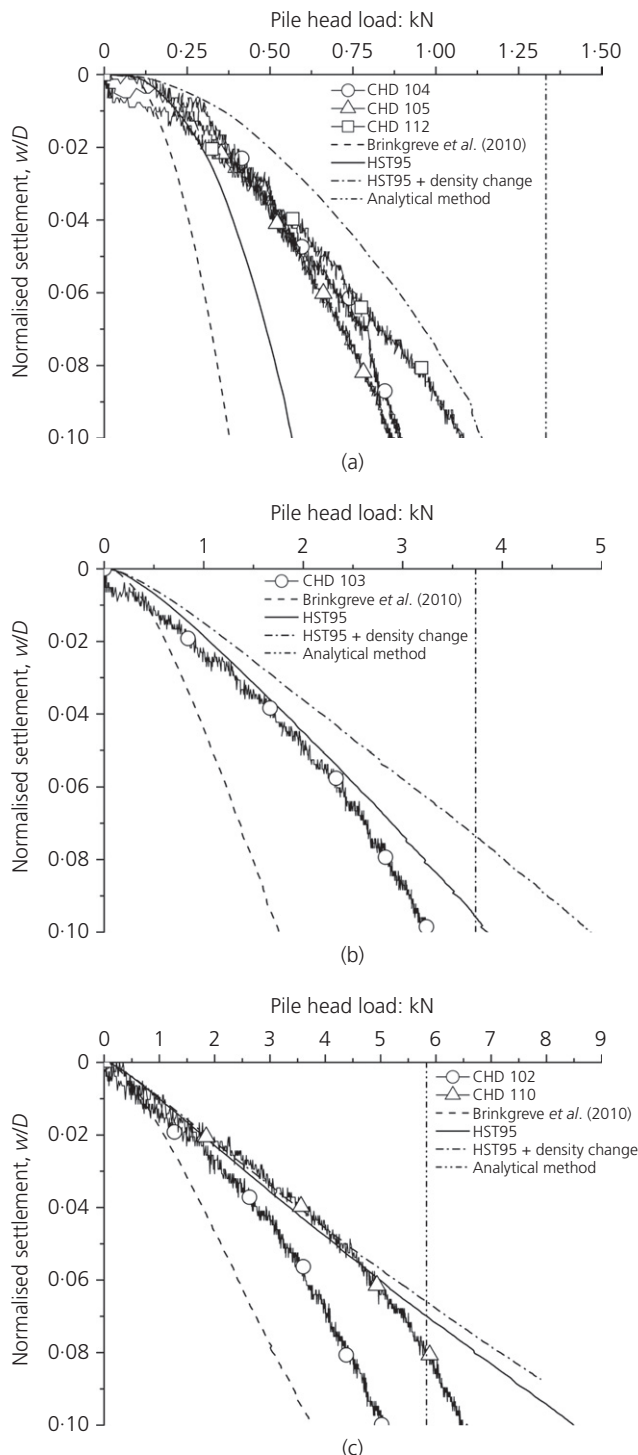
Figure 8. Pile head load–settlement prediction up to 10% diameter for CHD pile in (a) loose sand ($D_r = 17\%$), (b) medium dense sand ($D_r = 59\%$) and (c) dense sand ($D_r = 78\%$)

the predicted curve consistently slightly over-predicts the stiffness. Predictions using the HST95 parameters without changed densities under-predict in the loose case, are very

close for the medium case and over-predict in the dense case (giving a virtually indistinguishable result from the changed density model in Figure 8(c)). The consistency in the performance of the 'density change' cases would appear to suggest that it is important to account for these changes in soil state; the consistent over-prediction may suggest that there is some other non-density related disturbance to the soil properties due to the 1g model installation process. This will be revisited later in the paper when simulating the field pile cases that used the actual field installation procedure at full confining stress levels.

Considering the capacity predictions of the analytical model, it can be seen that, in the two denser cases, the analytical model gives a good estimation of the model test capacity and is conservative compared with the FEM at this point. In the loosest case, the analytical method over-predicts the measured load test data, while the FEM gives a much closer estimation. Figure 8 also suggests that if the relatively simple and rapid two-dimensional axisymmetric FEM analyses proposed here are used to obtain full load–settlement curves, they should be limited by the pile capacity obtained from the analytical model where this is less than the FEM capacity at $w/D = 0.1$. This may alternatively be expressed as the FEM being best used for determining performance at the serviceability limiting state (i.e. evaluation of settlement under working load, which would typically be less than or equal to half of the pile's bearing capacity), with the analytical model being used at the ultimate limiting state. This has the added advantage that the analytical model is easier to manipulate for the purposes of pile sizing (e.g. determining an appropriate length to give a suitable factor of safety (FoS)) and the more sophisticated FEM can be reserved for checking the serviceability of the resulting pile designs, thereby limiting the amount of this type of work that must be conducted.

As further validation, the split of the load carrying between base and shaft is presented in Figure 9. Figure 9(a) shows the load carried at the base of the pile (Q_b) normalised by the total load at the pile head (Q_t) from the FEM simulations. Firstly, it can be seen that the model CHD piles appear to act predominantly as frictional piles, carrying only 20–25% of the load at the pile tip. This is different to fully driven piles, which tend to be predominantly end bearing, but is consistent with the comments made in the companion paper (and here in Equation 5) that the base capacity is determined using the smaller core diameter. Secondly, under small-scale 1g test conditions, the shaft and base components are also mobilised at the same rate with respect to increasing settlement, as Q_b/Q_t is approximately constant throughout the simulations. Typically, shaft capacity would mobilise more quickly than base, resulting in an increasing value of Q_b/Q_t as settlement increases. However, at reduced scale, the mobilisation of base capacity will scale down with the tip diameter of the pile (bearing capacity mechanism), while the mobilisation distance in
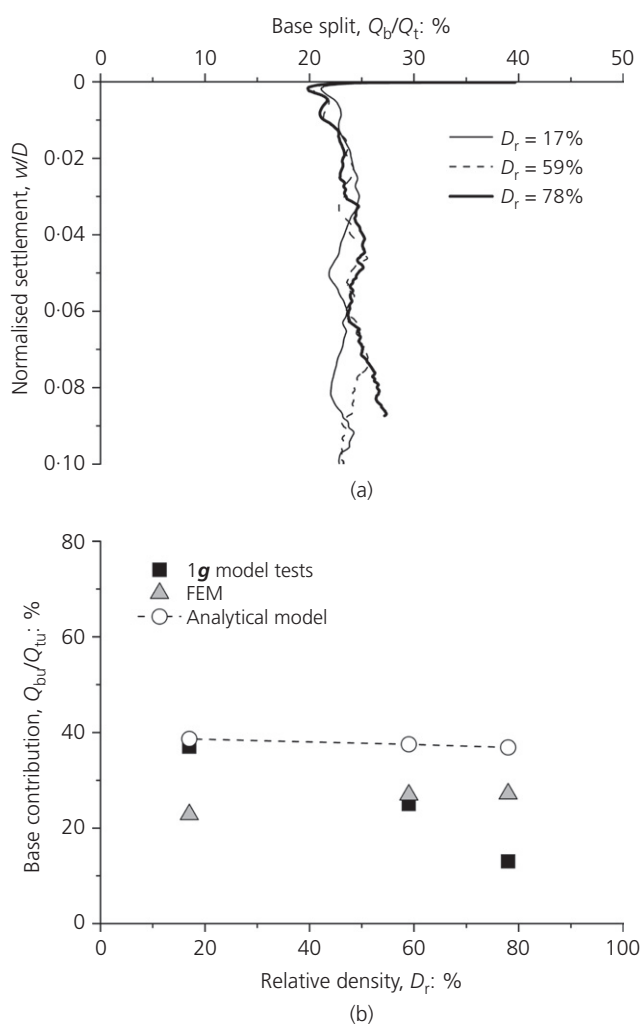
Figure 9. Split between base and shaft components of load
carrying in 1**g** model tests: (a) normalised mobilised base
contribution from FEM; (b) comparison of ultimate split at inferred
bearing capacity ($w/D = 0.1$ for FEM and model tests)

Project	Pile	Pile length, L: m	Number of CPTs	Approximate saturated unit weight, γ: kN/m^3
1	1·1	11·6	8	17
2	2·1	12·0	2	16
2	2·2	12·0	2	16
3	3·1	10·0	5	16

Table 2. Summary of available information for field CHD piles in
sandy ground

curves from compressive full-scale pile load tests of working
piles in sands. Four pile load test results, relating to piles instal-
led in coarse-grained materials were extracted from a larger
database of historical test data in a wide range of ground types
(Jeffrey, 2012). The four pile tests were conducted across three
projects/sites, hereafter termed projects 1, 2 and 3. Two piles
were tested within project 2. For each project, CPTs were con-
ducted during the initial ground investigation and these were
used to determine the variation of in situ relative density for
the selection of the constitutive model parameters in the FEM
simulations (this is discussed later). The length of the test piles
and available test data are summarised in Table 2. This table
also includes the assumed saturated unit weight of the ground
from the ground investigations, which was necessary to allow
the vertical effective stresses to be estimated for interpreting
the CPT data.

4.2   Interpretation of CPT data
To simplify the model generation within the FEM, the ground
at each site was split into layers, each 1 m thick. Based on the
number of CPTs available at each site (Table 2), an average
(mean) value of CPT cone resistance (q_c) was found for each
1 m thick layer. The average q_c and interpreted ground profiles
from the ground investigation reports are shown in Figure 10.
The vertical effective stress (σ'_v) at the centre of each layer was
then determined from the soil unit weight (γ) (Table 2) and the
known position of the water table. The relative density in each
layer was determined using

7. $$D_r = -1.21 + 0.584 \log\left(\frac{q_c}{\sigma_v'^{0.5}}\right)$$

Equation 7, taken from Knappett and Craig (2012), is based
on empirical fitting to a large database of CPTs conducted by
Jamiolkowski *et al.* (2001) and Mayne (2007). The relative
density in each layer was then used to estimate the constitutive
model parameters for the FE model using both the HST95
and Brinkgreve *et al.* (2010) correlations.

Predictions of the ultimate capacity of the piles were also made
using the analytical model procedures developed in the

shear (relative pile–soil vertical displacement) will not change
with diameter. Figure 9(b) compares Q_{bu}/Q_{tu} (i.e. the ratio
of Q_b/Q_t at $w/D = 0.1$) for the model tests (strain gauged piles),
the analytical model and FEM. It can be seen that all the
data support the notion of CHD piles acting as predominantly
frictional. The FEM values are in very close agreement with
the Q_{bu}/Q_{tu} values obtained from the model tests, while the
analytical model provides estimates at the upper end of the
range of Q_{bu}/Q_{tu} observed in the model tests.

4.   Application of FEM to field pile load tests

4.1   Overview of field test data
Following validation against the 1**g** small-scale model tests
described in the previous section, FEM procedures were sub-
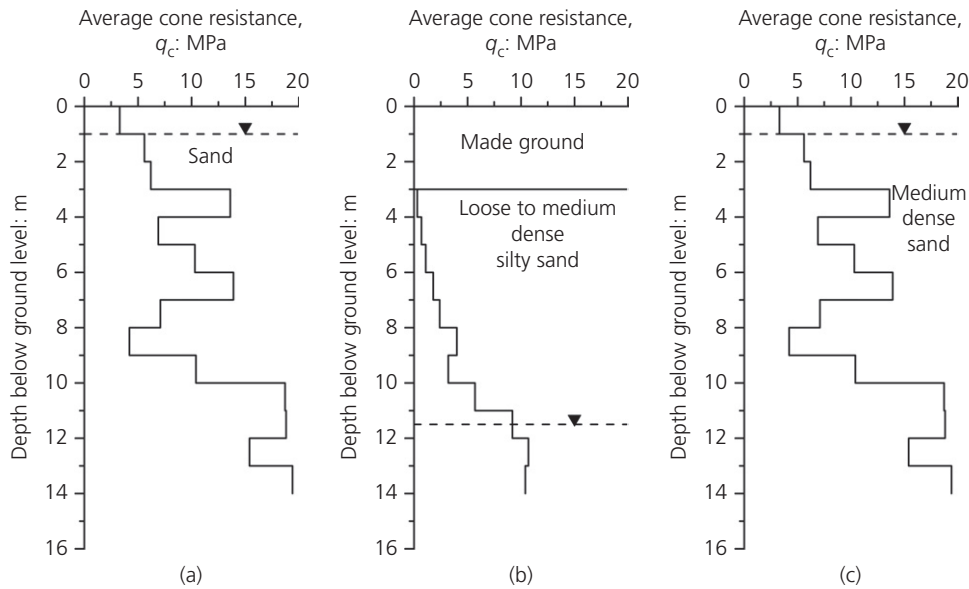sequently applied to the prediction of the load–settlement

Figure 10. Interpreted average cone resistance (q_c) and ground profiles for (a) project 1, (b) project 2 and (c) project 3

companion paper (Jeffrey *et al.*, 2016), for which the peak friction angle was required. These were determined directly from the CPT resistance using

8. $$\phi'_p = 6 \cdot 6 + 11 \log \left(\frac{q_c}{\sigma_v'^{0\cdot5}} \right)$$

also after Knappett and Craig (2012), based on data collated by Mayne (2007). The derived soil parameters at each site are presented alongside the predicted load–settlement behaviour from the FEM and capacities from the analytical model for each case study separately in Sections 4.4–4.6.

4.3   General modelling considerations

As the load tests considered here were conducted on working piles, it was not possible to exhume them to measure the actual geometry of the piles produced. Instead, an idealised geometry, shown in Figure 11 was used based on the exterior geometry of the full-scale CHD bullet and assuming a perfect pile is produced. D_{core} (= 0·3 m from Figure 11) was used to determine the base capacity, as for the model tests. This was then surrounded by a mesh of soil elements as shown in Figure 12. This mesh was produced in 1 m thick layers such that the constitutive parameters could be varied every metre (based on the derived relative density from the CPT investigations at each site, as described in the previous section) and thereby approximately capture the natural variation in the soil properties with depth, without requiring an excessive amount of data input.
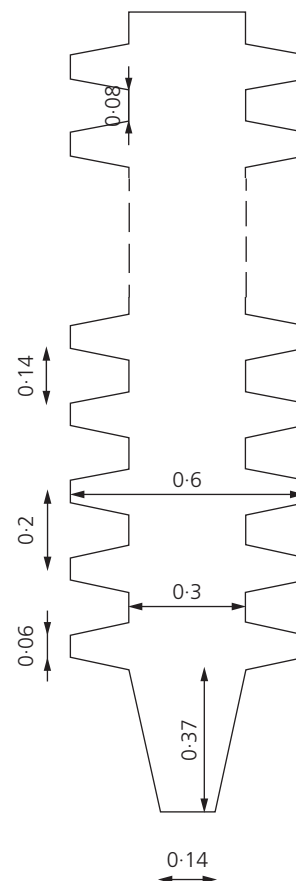

Figure 11. Idealised CHD pile geometry used in FEM of field CHD piles (all dimensions shown in m)
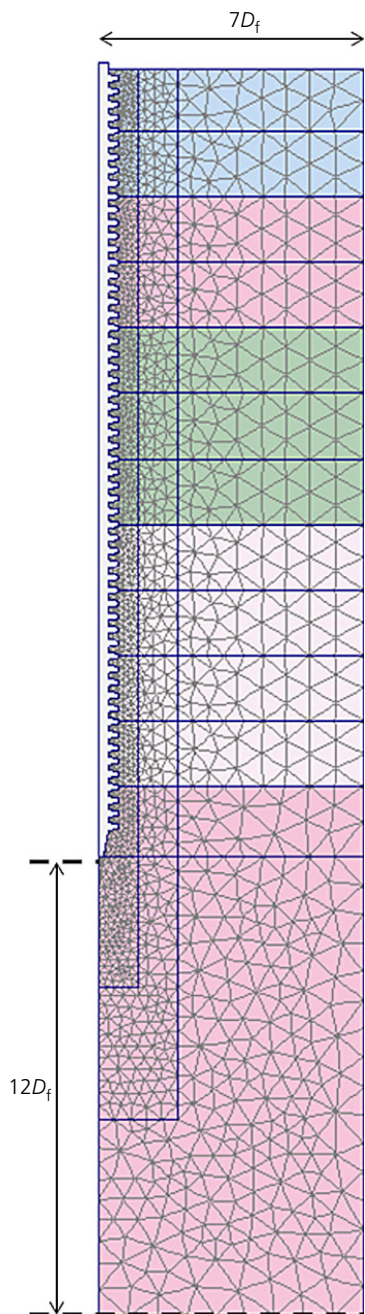
Figure 12. Model domain and mesh configuration for FEM of field CHD piles

Figure 13. Illustration of simplification of variation of radial soil properties

that, as an approximation, in medium-density soils the soil density is unchanged or perhaps slightly reduced over the upper third of the pile, and increased below this depth by up to 20%, depending on the radial distance from the pile. As with the discretisation of soil properties with depth, the radial variation of soil properties was simplified as shown in Figure 13, where D_r, the pre-installation in situ relative density (i.e. that determined by applying Equation 7 to the CPT data), is modified in different zones of the FE model. These density modifications were applied to all of the field simulations conducted (i.e. for both the HST95 and Brinkgreve *et al.* (2010) parameter sets).

4.4 Results: project 1
Figure 14(a) shows the results of the CPT data interpretation for project 1. It can be seen that the site consists of 2 m of relatively loose sand overlying a deep deposit of relatively uniform medium dense sand ($D_r \approx 50\%$). The interpreted friction angles derived from the CPT data (Equation 8) very closely match those used in the HST95 constitutive model parameter set, suggesting that this may be more appropriate in this case than the model proposed by Brinkgreve *et al.* (2010).

Figure 14(b) shows the load test data measured in the field test (constant rate of penetration, CRP), with load–settlement predictions from FEM and the analytically predicted bearing capacity. It was not possible to take the FEM simulations fully to $0·1D_f$ due to excessive distortion occurring in the mesh.

It has been discussed earlier how the installation of CHD piles in sand may be approximated within FEM in relation to the 1:10 scale model tests. For these earlier simulations it was possible to incorporate the apparent density changes within the FEM in detail (see Figures 6 and 7) as they were measured by post-installation model CPTs conducted close to the pile. However, these data were not available for the field piles and would in any case be expensive to determine. Figure 7 suggests
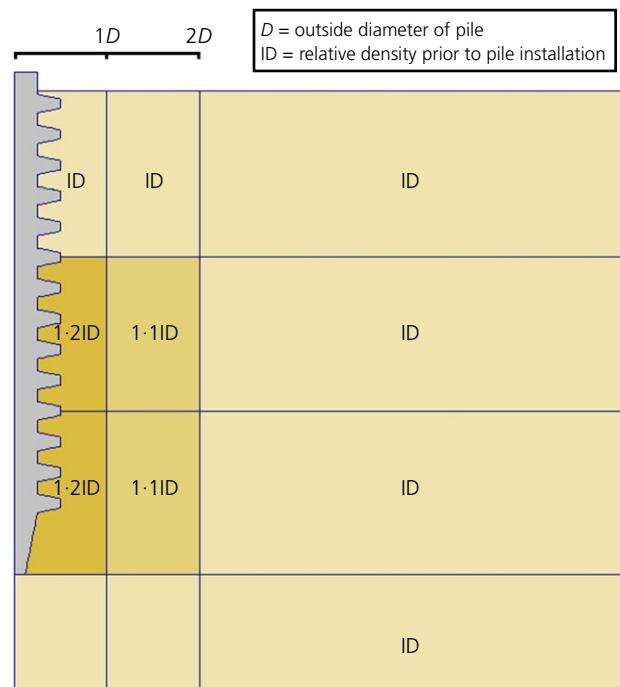
Figure 14. (a) Derived input parameters from in situ CPT data for project 1. (b) Results of FEM and bearing capacity prediction compared with measured field pile tests

However, extrapolation of the curves over the final 10–15 mm of vertical movement would suggest that the simulations would reach the capacity predicted using the analytical method (which uses lower bound values of K as outlined in the companion paper) at $w/D = 0.07$. The pile load tests were limited to 150% of working load, so it is not possible to validate fully the

analytical capacity predictions against the pile load test data. However, in terms of serviceability-based performance, both FEM simulations under-predict the axial stiffness of the test pile, with the HST95 model giving a better estimation. This would be conservative when used to design a CHD pile to meet a certain limiting settlement, but might be unconservative in terms of the induced structural loads if the load–settlement curve from the FEM was used to model a non-linear foundation spring as part of a soil–structure interaction analysis. There is some apparent stiffening of the curve for $w > 30$ mm ($0.05D_f$ or approximately half of the maximum simulation displacement), which is thought to be due to some distortion of the mesh in the small zones between the flanges, which are small compared to the outer (flange) diameter of the pile, and therefore will begin to distort at lower settlements compared to the mesh around the pile. However, the load that would induce this settlement is 70% of the ultimate capacity, implying that this would not be an issue if the FEM is used to determine settlements in the working load range for piles with an overall FoS > 1·4. A similar feature was noted in the simulations of subsequent projects.

4.5   Results: project 2
Figure 15(a) shows the results of the CPT data interpretation for project 2. This site is more complex than project 1, consisting of 3 m of made ground in which there were no CPT data, overlying silty sand having a density that increases with depth. In this case, the interpreted friction angles derived from the CPT data match more closely with the Brinkgreve *et al.* (2010) parameter set, which give lower values. For the made ground, it was assumed that the soil can be treated as sand with a density equivalent to that between 3–5 m below ground level (i.e. assuming the material has relatively low strength and stiffness). It should be noted that, in any case, the material around the top of the pile is only likely to provide a small contribution to the pile stiffness and bearing capacity, due to the lower confining stress at these depths. Figure 15(b) shows the load test data measured in the field tests, with load–settlement predictions from FEM and the analytically predicted bearing capacity. For this project, the HST95 and Brinkgreve *et al.* (2010) curves give very similar and very good predictions of the average of the two load tests, at least up to a load of 750 kN; however, beyond this (up to the maximum test load) the Brinkgreve *et al.* (2010) method increasingly under-predicts the stiffness compared with the HST95 simulation, as also observed for project 1. Extrapolation of the HST95 curve is consistent with the prediction from the analytical bearing capacity method, with the FEM curve reaching this capacity at $w/D = 0.08$.

4.6   Results: project 3
Figure 16(a) shows the results of the CPT data interpretation for project 3. This site consists of sand that is generally denser than that at project 1, with greater variability over the length of the pile. As for project 1, the interpreted friction angles

derived from the CPT data (Equation 8) more closely match those used in the HST95 constitutive model parameter set, suggesting that the FEM simulation with this parameter set will be most appropriate in this case. Figure 16(b) shows the load test data measured in the field test, with load–settlement predictions from FEM and the analytically predicted bearing capacity. Similarly to project 1, the FEM curve for the HST95 parameter set is closer to the load test data than that using the Brinkgreve *et al.* (2010) curve. Extrapolation of the HST95 curve would suggest that the simulations would reach the capacity predicted using the analytical method at $w/D = 0.06$.

4.7   Base–shaft load split
Figure 17(a) shows data from the FEM simulations (HST95 parameter set) relating to the base–shaft load split. At full-scale stress levels, the CHD piles act more in shaft friction than in the reduced scale model tests, with the base contributing 10–20% of the capacity at an extrapolated $w/D = 0.1$. It can also be seen that, at these higher stress levels, the shaft capacity mobilises over small deformations: Q_b/Q_t is constant up to $w/D \approx 0.005$ or $w \approx 3$ mm, which is of similar order of magnitude to $w = 6$ mm for the complete 1:10 scale load test (see Figure 9). After this point, the base provides an increasingly larger component of the total load carrying, suggesting that the shaft component has reached a limiting value. This is more typical of displacement pile behaviour, but Q_{bu}/Q_{tu} is still relatively small given the small size of D_{core} compared with D_{shaft}. Figure 17(b) compares the ultimate load split with that predicted from the analytical model (as field measurements of base loads were not possible in the working piles). The latter suggests larger contributions of the tip; however, both methods clearly indicate the predominantly frictional nature of the pile behaviour.

5.   Implications for the design of CHD piles
The overall aim of conducting the physical model testing presented in the companion paper (Jeffrey *et al.*, 2016) and the accompanying numerical simulation described in this paper was to develop improved simple design approaches for CHD piles that remove at least some of the conservatism in current design approaches. The physical modelling from the companion paper was used to present appropriate design parameters for predicting bearing capacity, and the numerical modelling outlined in this paper suggested that this method would give appropriate predictions when applied to field-scale piles. This approach will be particularly useful when performing initial sizing of a CHD pile (i.e. determining its length, as the bullet diameter typically only has a small range of sizes) to provide a certain overall FoS or to satisfy the ultimate limit state with a particular combination of partial factors. Once initial sizing is complete, the FEM procedures outlined in this paper can be used to determine the performance (settlement) under working loads to confirm that serviceability criteria are expected to be met. Figures 14(b)–16(b)
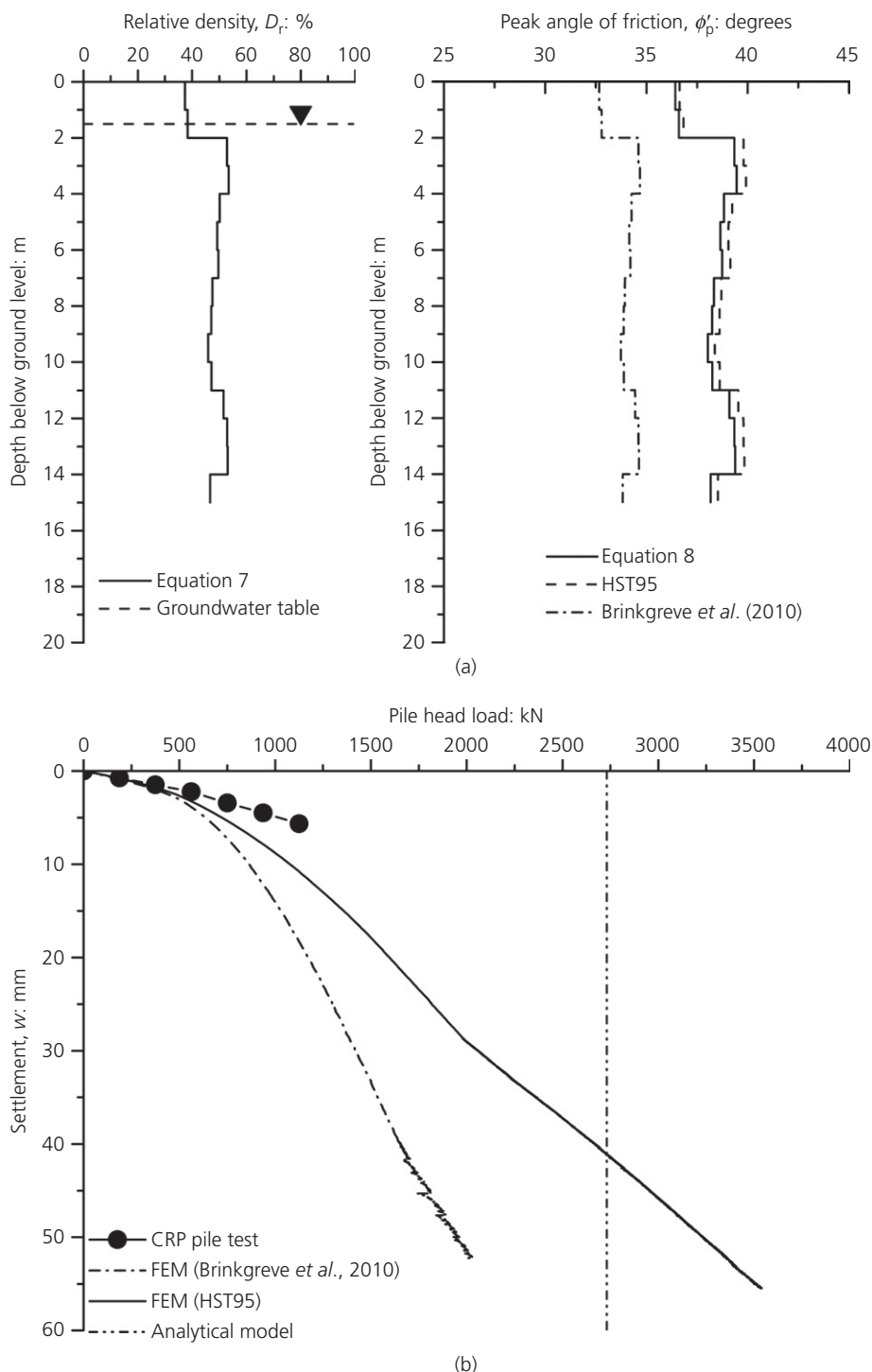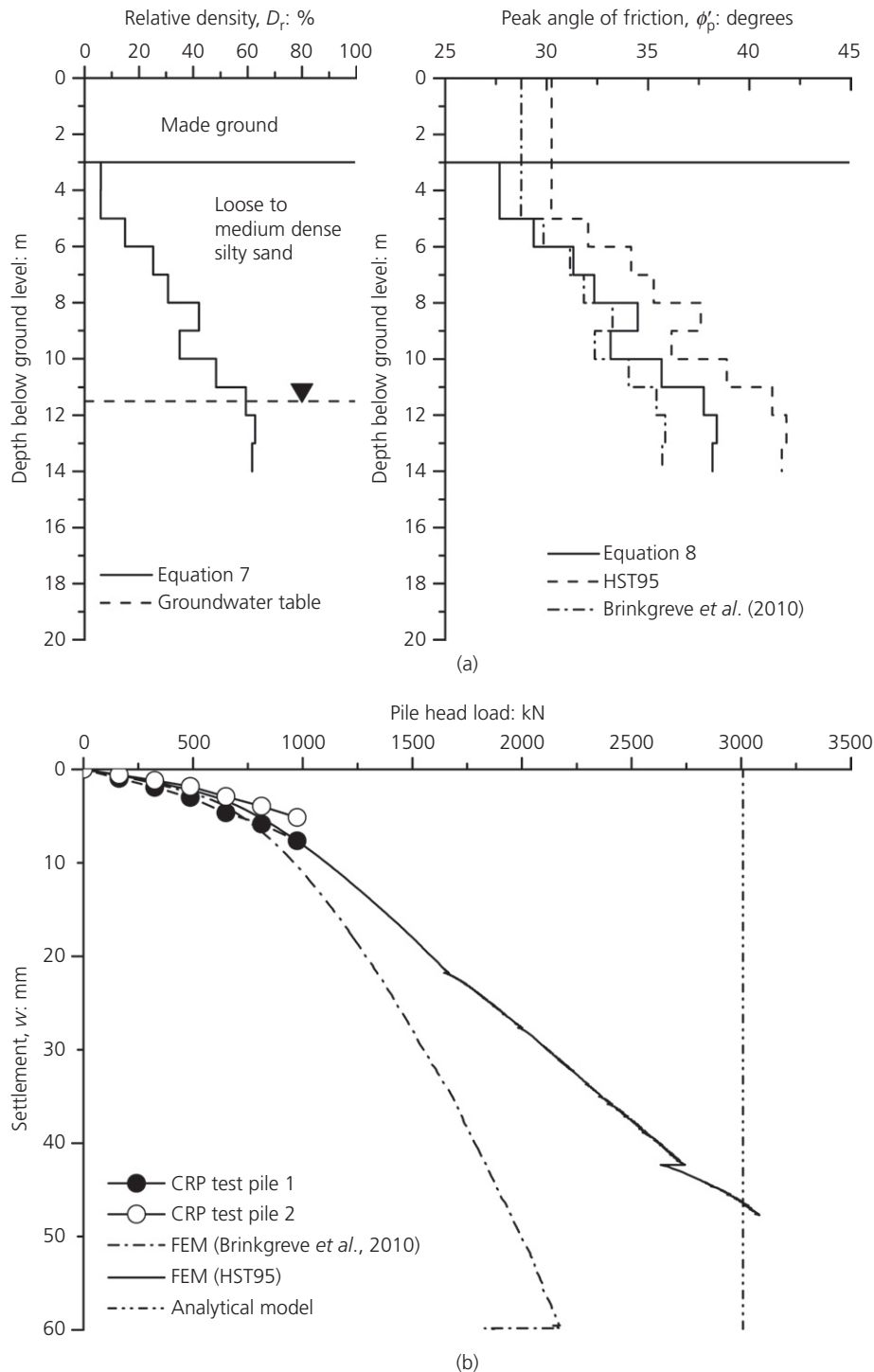
Figure 15. (a) Derived input parameters from in situ CPT data for
project 2. (b) Results of FEM and bearing capacity prediction
compared with measured field pile tests

would suggest that such estimates will be conservative with regard to settlements at working loads and will therefore lead to acceptable pile designs. A comparison of the performance of the FEM methods against the load test data is provided in Table 3 (at working load) and Table 4 (at maximum test load).
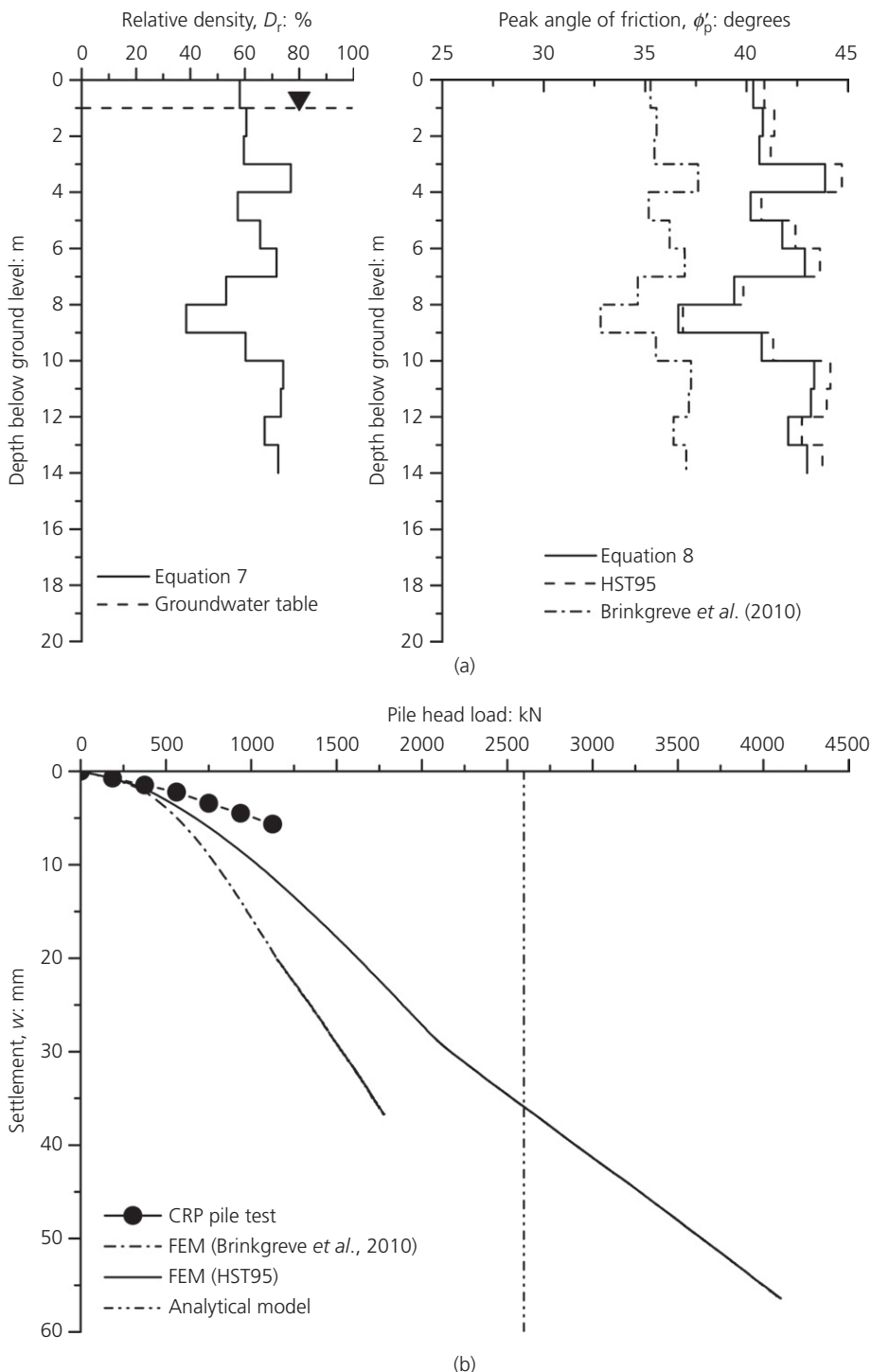
Figure 16. (a) Derived input parameters from in situ CPT data for project 3. (b) Results of FEM and bearing capacity prediction compared with measured field pile tests

To demonstrate the benefit of the FEM procedures further, predictions of pile settlement at working and maximum test loads were also made using the popular method of Fleming (1992), including elastic shortening effects, and these are also shown in Tables 3 and 4. In performing these calculations, the shaft and base diameters were taken as D_f and D_{core}, respectively
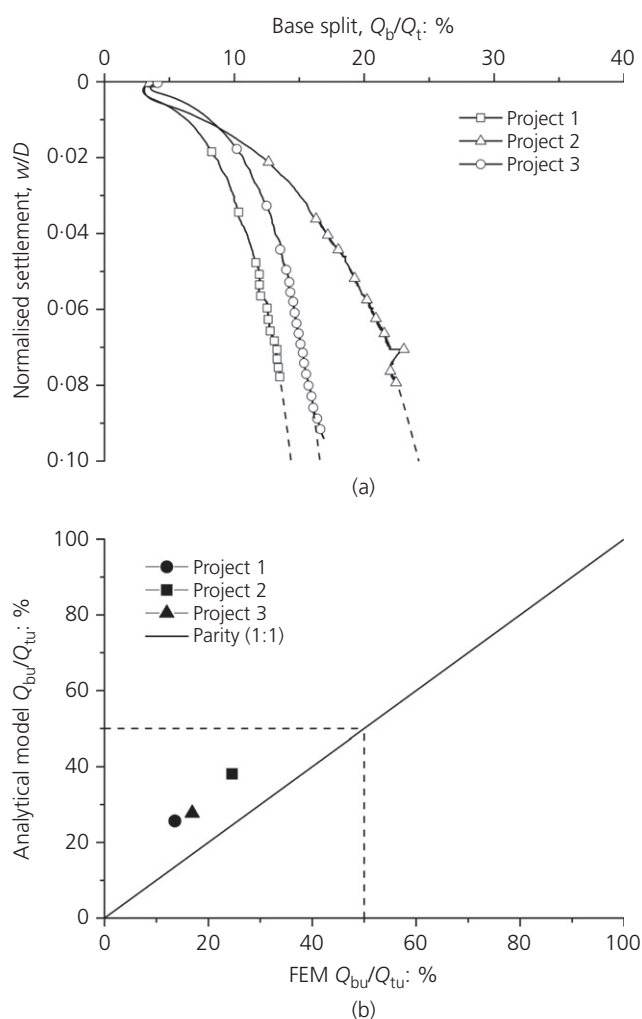
Figure 17. Split between base and shaft components of load carrying in field cases: (a) normalised mobilised base contribution from FEM; (b) comparison of ultimate split at inferred bearing capacity ($w/D = 0.1$ for FEM)

(i.e. the same assumptions as the analytical model), the pile lengths were from Table 2 and the shaft and base capacities were computed using the analytical model from the companion paper (these capacities are included in Table 5). Fleming's method also requires three stiffness parameters – namely, Young's modulus of the concrete E_c (based on the range of 24–28 GPa reported by Brown *et al.* (2006)), the shaft–soil flexibility factor M_s (0·001–0·004, after Fleming (1992)) and Young's modulus of the soil at the pile base E_b (30–100 MPa for medium dense sand, after Azizi (1999)). In Tables 3 and 4, a range is given for these predictions – the smallest settlement represents the stiffest combination ($E_c = 28$ GPa, $M_s = 0.004$, $E_b = 100$ MPa) and the largest settlement represents the most flexible combination ($E_c = 24$ GPa, $M_s = 0.001$, $E_b = 30$ MPa).

It can be seen from Tables 3 and 4 that Fleming's method under-predicts the settlement in all cases. In contrast, except in one case (pile 2.1) the FEM methods over-predict settlements, which would be a more desirable outcome in terms of having increased confidence that the piles as designed would meet tolerable settlement requirements at the serviceability limit state. It should also be noted that both the simple capacity determination method and the non-linear FEM only require basic soil data for their use, specifically ϕ'_p for the capacity method and D_r for the FEM. Both of these parameters can be determined using CPT (or standard penetration test) testing, which is already routinely used in pile design. In contrast, Fleming's method requires the estimation of E_b and M_s. While these parameters could be back-calculated from a pile load test (as suggested by Fleming (1992)), they are difficult to determine a priori from routine ground investigation.

The new approaches outlined here and in the companion paper will allow pile designers to be more confident in using more of the available pile capacity in design, thereby reducing the amount of material required to support a given load or meet a required serviceability criterion, thereby reducing cost and improving sustainability. As an example, the actual

Pile	Applied load: kN	*w*: mm			
		Measured	FEM (HST95)	FEM (Brinkgreve *et al.*, 2010)	Analytical (Fleming, 1992)
1·1	750	3·43	5·33 (+55%)	7·23 (+111%)	1·08 to 2·21 (−69% to −36%)
2·1	650	4·64	3·37 (−27%)	4·00 (−14%)	0·97 to 2·00 (−79% to −57%)
2·2	650	2·92	3·37 (+15%)	4·00 (+37%)	0·97 to 2·00 (−67% to −32%)
3·1	600	3·69	4·15 (+12%)	5·65 (+53%)	0·78 to 1·68 (−79% to −54%)

Table 3. Comparison of settlements measured in load tests with predictions from FEM and an existing analytical model at working load

16

Pile	Applied load: kN	w: mm			
		Measured	FEM (HST95)	FEM (Brinkgreve *et al.*, 2010)	Analytical (Fleming, 1992)
1·1	1125	5·65	10·78 (+ 91%)	18·32 (+ 224%)	1·80 to 4·50 (− 68% to − 20%)
2·1	975	7·64	7·65 (+ 0%)	10·34 (+ 35%)	1·61 to 3·60 (− 79% to − 53%)
2·2	975	5·14	7·65 (+ 49%)	10·34 (+ 101%)	1·61 to 3·60 (− 69% to − 30%)
3·1	900	5·45	8·00 (+ 47%)	12·82 (+ 135%)	1·29 to 2·96 (− 76% to − 46%)

Table 4. Comparison of settlements measured in load tests with predictions from FEM and an existing analytical model at maximum test load

Pile	L: m	Q_{bu}: kN	Q_{su}: kN	Q_{tu}: kN	Working load: kN	'Actual' FoS	Reduction in length (FoS = 2·5): %
1·1	11·6	701	2030	2731	750	3·6	22
2·1, 2·2	12·0	1147	1861	3008	650	4·6	19
3·1	10·0	720	1877	2597	600	4·3	38

Table 5. Potential reductions in pile length that could have been realised for the piles on projects 1–3 using the new methods

overall factors of safety designed into the field piles using existing methods were evaluated using the estimates of pile capacity from the analytical model and assuming this to be the 'actual' bearing capacity. The new method was used to estimate the length of pile required to meet a target overall FoS of 2·5. It should be noted that this FoS could represent either a selected value as in traditional pile design, or could relate to a pile designed to limit state design principles, where the combination of characteristic material property selection and partial action, material and resistance factors results in a pile having an allowable design load 2·5 times smaller than the characteristic pile resistance. By comparing this new length to that actually constructed it is possible to demonstrate the potential savings that could be made in material costs and embodied carbon dioxide (both of which would be influenced by the pile length) by using the new methods, assuming that there were no other constraints on the minimum pile length. The results of these calculations are summarised in Table 5. These calculations were subsequently repeated for different target FoS values between 2·5 and the 'actual' capacity determined using the new methods for the as-built lengths to show that savings in pile length can be made even if a more conservative FoS is desired in design. The results are shown in Figure 18. It can be seen that existing design methods appear to have resulted in field piles with a FoS of 3·6–4·6 (Table 5). Savings in material costs and installation time could be particularly significant on projects where there are many tens or hundreds of piles to install and, as noted before, in using the
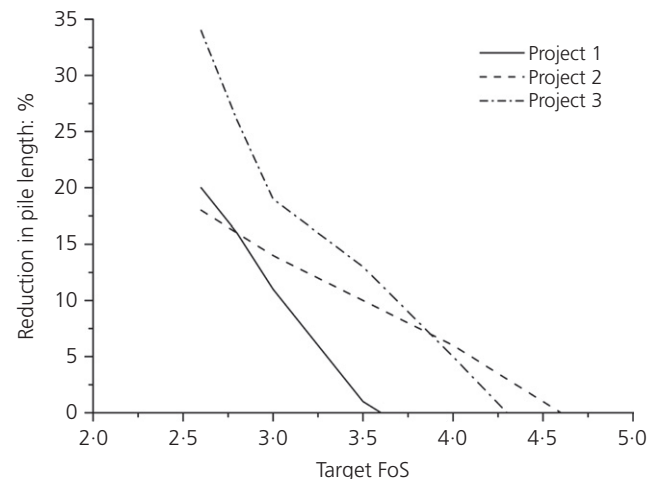

Figure 18. Potential for material savings compared with existing design techniques for CHD piles

new methods there are no additional costs in terms of additional ground investigations or more advanced laboratory testing beyond those that would usually be required.

6. Conclusions
Commercially available non-linear FEM has been applied to the simulation of compressive pile load tests of continuous

17

helical displacement (CHD) piles in sands from both 1:10 scale 1*g* model tests (reported in the companion paper (Jeffrey *et al.*, 2016)) and in field tests of four working (field) piles at three different sites. It has been shown that a reasonable prediction of the load–settlement behaviour at typical working load levels (i.e. serviceability limiting state) can be achieved using an advanced non-linear constitutive model that can be fully parameterised using basic soil data available from routine geotechnical site investigation data (e.g. cone penetration tests) without the need to employ large deformation modelling techniques. When combined with the analytical capacity prediction method (i.e. ultimate limit state) developed in the companion paper, this suggests that savings in terms of pile length/material could potentially be made when designing future CHD piles due to the increased confidence in capacity and settlement prediction that the new methods provide.

Acknowledgements

REFERENCES

Al-Defae AH, Caucis K and Knappett JA (2013) Aftershocks and the whole-life seismic performance of granular slopes. *Géotechnique* **63(14)**: 1230–1244, http://dx.doi.org/10.1680/geot.12.P.149.

Azizi F (1999) *Applied Analyses in Geotechnics.* Taylor & Francis, Abingdon, UK.

Brinkgreve RBJ, Engin E and Engin HK (2010) Validation of empirical formulas to derive model parameters for sands. In *Numerical Methods in Geotechnical Engineering* (Benz T and Nordal S (eds)). CRC Press/Balkema, Rotterdam, the Netherlands, pp. 137–142.

Brown MJ, Hyde AFL and Anderson WF (2006) Analysis of a rapid load test on an instrumented bored pile in clay. *Géotechnique* **56(9)**: 627–638, http://dx.doi.org/10.1680/geot.2006.56.9.627.

BSI (2004) BS EN 1997-1:2004: Eurocode 7: geotechnical design – part I: general rules. BSI, London, UK.

Fleming WGK (1992) A new method for single pile settlement prediction and analysis. *Géotechnique* **42(3)**: 411–425, http://dx.doi.org/10.1680/geot.1992.42.3.411.

Hardin BO and Drnevich VP (1972) Shear modulus and damping in soils: design equations and curves. *ASCE Journal of Soil Mechanics and Foundations Division* **98(SM7)**: 667–692.

Jamiolkowski M, LoPresti DCF and Manassero M (2001) Evaluation of relative density and shear strength of sands from cone penetration test and flat dilatometer test. In *Soil Behavior and Soft Ground Construction* (Germaine JT, Sheahan TC and Whitman RV (eds)). ASCE, Reston, VA, USA, Geotechnical Special Publication 119, pp. 201–238.

Jeffrey J, Brown MJ, Knappett JA, Ball J and Caucis K (2016) CHD pile performance: part I – physical modelling. *Proceedings of the Institution of Civil Engineers – Geotechnical Engineering*, http://dx.doi.org/10.1680/jgeen.15.00131.

Jeffrey JR (2012) *Investigating the Performance of Continuous Helical Displacement Piles.* PhD thesis, Division of Civil Engineering, University of Dundee, Dundee, UK.

Katzenbach R and Schmitt A (2005) Bored and screwed piles. In *Proceedings of the 16th International Conference on Soil Mechanics and Geotechnical Engineering, Osaka, Japan* (Adachi A (ed.)). Millpress, Rotterdam, the Netherlands, vol. 4, pp. 2129–2132.

Knappett JA and Craig RF (2012) *Craig's Soil Mechanics*, 8th edn. Taylor & Francis, Abingdon, UK.

Knappett JA, Madden P and Caucis K (2015) Seismic structure–soil–structure interaction between pairs of adjacent building structures. *Géotechnique* **65(5)**: 429–441, http://dx.doi.org/10.1680/geot.SIP.14.P.059.

Kulhawy FH (1984) Limiting tip and side resistance, fact or fallacy? *Proceedings of ASCE Symposium on Analysis and Design of Pile Foundations, San Francisco, CA, USA*, pp. 80–98.

Kurian NP and Shah SJ (2009) Studies on the behaviour of screw piles by the finite element method. *Canadian Geotechnical Journal* **46(6)**: 627–638.

Liang T, Knappett JA and Duckett N (2015) Modelling the seismic performance of rooted slopes from individual root-soil interaction to global slope behaviour. *Géotechnique* **65(12)**: 995–1009, http://dx.doi.org/10.1680/geot.14.P.207.

Mayne PW (2007) *Cone Penetration Testing: A Synthesis of Highway Practice.* Transportation Research Board, Washington, DC, USA, NCHRP Synthesis Report 368.

Oztoprak S and Bolton MD (2013) Stiffness of sands through a laboratory test database. *Géotechnique* **63(1)**: 54–70, http://dx.doi.org/10.1680/geot.SIP.10.P.078.

Santos JA and Correia AG (2001) Reference threshold shear strain of soil – its application to obtain a unique strain-dependent shear modulus curve for soil. *Proceedings of the 15th International Conference on Soil Mechanics and Geotechnical Engineering, Istanbul, Turkey*, vol. 1, pp. 267–270.

Schanz T, Vermeer PA and Bonnier PG (1999) The hardening-soil model: formulation and verification. In *Beyond 2000 in Computation Geotechnics* (Brinkgreve RBJ (ed.)). Balkema, Rotterdam, the Netherlands, pp. 281–290.

Tolooiyan A and Gavin K (2013) The base resistance of non-displacement piles in sand. Part II: finite-element

analyses. *Proceedings of the Institution of Civil Engineers – Geotechnical Engineering* **166(6)**: 549–560, http://dx.doi.org/10.1680/geng.11.00101.

Wehnert M and Vermeer PA (2004) Numerical analyses of load tests on bored piles. In *Proceedings of the 9th International Symposium on Numerical Methods in Geomechanics (NUMOG IX), Ottawa, Canada* (Pande GN and Pietruszczak S (eds)). Balkema, Rotterdam, the Netherlands, pp. 505–511.

WHAT DO YOU THINK?

To discuss this paper, please email up to 500 words to the editor at journals@ice.org.uk. Your contribution will be forwarded to the author(s) for a reply and, if considered appropriate by the editorial panel, will be published as discussion in a future issue of the journal.

Proceedings journals rely entirely on contributions sent in by civil engineering professionals, academics and students. Papers should be 2000–5000 words long (briefing papers should be 1000–2000 words long), with adequate illustrations and references. You can submit your paper online via www.icevirtuallibrary.com/content/journals, where you will also find detailed author guidelines.